The Astrophysical Journal Letters, 866:L16 (6pp), 2018 October 20 https://doi.org/10.3847/2041-8213/aae51b

Delayed Jet Breakouts from Binary Neutron Star Mergers

Tatsuya Matsumoto[1,2,6] and Shigeo S. Kimura[3,4,5]
[1] Racah Institute of Physics, Hebrew University, Jerusalem, 91904, Israel; tatsuya.matsumoto@mail.huji.ac.il
[2] Department of Physics, Graduate School of Science, Kyoto University, Kyoto 606-8502, Japan
[3] Department of Physics, The Pennsylvania State University, University Park, PA 16802, USA
[4] Department of Astronomy & Astrophysics, The Pennsylvania State University, University Park, PA 16802, USA
[5] Center for Particle and Gravitational Astrophysics, The Pennsylvania State University, University Park, PA 16802, USA
Received 2018 September 2; revised 2018 September 24; accepted 2018 September 28; published 2018 October 12

Abstract

Short gamma-ray bursts (sGRBs) are thought to be produced by binary neutron star mergers. While an sGRB requires a relativistic jet to break out of ejecta, the jet may be choked and fails to produce a successful sGRB. We propose a "delayed breakout" scenario where a late-time jet launched by a long-term engine activity can penetrate ejecta even if a prompt jet is choked. Observationally, such a late-time jet is supported by the long-lasting high-energy emissions in sGRBs. Solving the jet propagation in ejecta, we show that a typical late-time activity easily achieves the delayed breakout. This event shows not prompt γ-rays but long-time X-ray emissions for $\sim 10^{2-3}$ s or even $\sim 10^{4-5}$ s. Some delayed events may be already detected as soft-long GRBs without supernova signatures. In an optimistic case, a few events coincident with gravitational-waves (GWs) are detected by the second-generation GW detectors every year. X-ray follow-ups of merger events without γ-rays will be a probe of long-lasting engine activities in binary mergers.

Key words: gamma-ray burst: general – gravitational waves – stars: black holes – stars: jets – stars: neutron

1. Introduction

Short gamma-ray bursts (sGRBs) are a class of gamma-ray bursts (GRBs) whose duration is less than 2 s (see Nakar 2007; Berger 2014, for reviews). They are believed to be powered by relativistic jets launched from compact binary mergers (Eichler et al. 1989). This model is strongly supported by the detection of the gravitational waves (GWs) from the merging binary neutron star (NS; GW170817; Abbott et al. 2017) and by the extensive follow-ups of electromagnetic counterparts, especially very long baseline interferometry (VLBI) observations (Ghirlanda et al. 2018; Mooley et al. 2018).

Some binary–NS mergers may fail to produce sGRBs even if they launch relativistic jets. In order to produce an sGRB, the relativistic jet should break out of the matter ejected by the binary coalescence (Murguia-Berthier et al. 2014; Nagakura et al. 2014). When the ejecta are too massive or the jet opening angle is too large, the jet is choked and fails to emit prompt γ-rays. Choked-jet events are supported by a threshold timescale to produce sGRBs that appears in the duration distribution of sGRBs (Moharana & Piran 2017). Furthermore, the observed binary–NS merger rate larger than the local sGRB rate also suggests choked events.

In addition to prompt γ-rays, some (or most) sGRBs show long-lasting high-energy emissions (Kisaka et al. 2017). They are classified as an extended emission with the duration of $\sim 10^{2-3}$ s (Norris & Bonnell 2006) and a plateau emission with $\sim 10^{4-5}$ s (Gompertz et al. 2013, 2014). Because it is difficult to explain them using the standard afterglow theory (Ioka et al. 2005), their origins are attributed to prolonged central-engine activities that launch jets or outflows (Metzger et al. 2008; Nakamura et al. 2014; Kisaka & Ioka 2015).

Even if a prompt jet is choked, a late jet may penetrate ejecta.[7] Late-time jets can be more powerful than prompt ones because some extended emissions have larger amounts of energy than that of prompt emissions (e.g., Perley et al. 2009). The ejecta's expansion also helps the late jet to break out by reducing the ejecta density. Hereafter, we refer to this scenario as "delayed jet breakout." In Figure 1, we show a schematic picture. We calculate the propagation of the late-time jet in the ejecta and find that the delayed jet breakout is realized with a typical late-time engine activity. In such an event, we cannot detect prompt γ-rays because the prompt jet is choked. Instead, a late-time jet breaks out of ejecta $\gtrsim 10^{1-2}$ s after the merger, and produces extended and plateau emissions. This can be observed as a soft-long GRB. We also discuss the event rate of the delayed jet breakouts and argue that they might have been observed by the *Monitor of All-sky X-ray Image* (*MAXI*).

2. Jet Propagation in Expanding Media

We calculate the jet propagation in the ejecta of a binary–NS merger by using a semi-analytical formula along Bromberg et al. (2011; see also Margalit et al. 2018). A jet launched from a central engine collides with ejecta and produces a jet head and cocoon. The cocoon surrounds the jet and collimates it (see below). The jet head velocity is given by the momentum balancing at the head as (Matzner 2003; Bromberg et al. 2011)

$$\beta_{\rm h} = \frac{\tilde{L}^{1/2}\beta_{\rm j} + \beta_{\rm a}}{\tilde{L}^{1/2} + 1}, \tag{1}$$

$$\tilde{L} \simeq \frac{L_{\rm j}}{\Sigma_{\rm j}\rho_{\rm a}\Gamma_{\rm a}^2 c^3}, \tag{2}$$

where $\beta_{\rm j} \simeq 1$, $\beta_{\rm a}$, $L_{\rm j}$, $\Sigma_{\rm j}$, $\rho_{\rm a}$, $\Gamma_{\rm a} = (1-\beta_{\rm a}^2)^{-1/2}$, and c are the velocity of the jet material, ejecta velocity, one-sided jet luminosity,[8] jet cross section, ejecta density, ejecta's Lorentz

[6] JSPS Research Fellow.

[7] We do not specify whether a delayed jet is powered separately from a prompt jet (Metzger et al. 2008) or is the same as the prompt one but with reduced luminosity (Kisaka & Ioka 2015). For the latter case, after the prompt jet is choked, a prolonged energy injection from the engine may produce a jet head structure.

[8] This luminosity is written as $L_{\rm j} = \theta_{\rm j}^2 L_{\rm j,iso}/4$ by the jet opening angle $\theta_{\rm j}$ and isotropic jet luminosity $L_{\rm j,iso}$.

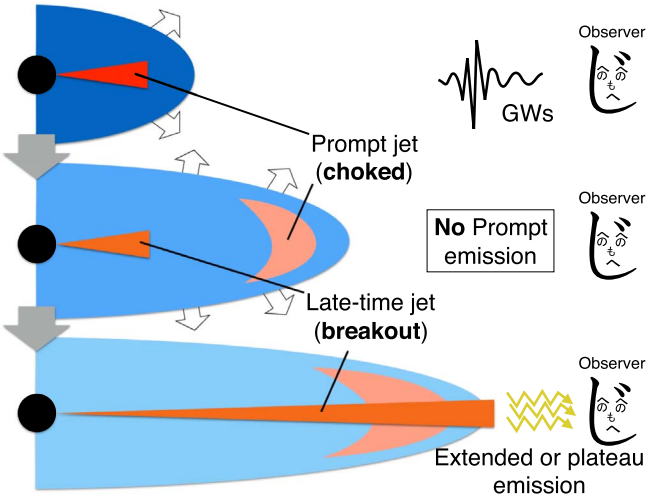

Figure 1. Schematic picture of a delayed-jet-breakout event. First, a prompt jet is choked and fails to produce an sGRB (top). Another jet that powers extended or plateau emission is launched later (middle). It is also possible that the delayed jet is identical to the prompt one but with reduced luminosity. Due to expansion, the ejecta density becomes tenuous and helps the late-time jet to break out of ejecta (bottom).

factor, and speed of light, respectively. The ejecta's quantities are evaluated at the head.

We assume that the ejecta are homologous and have a power-law density profile (Hotokezaka et al. 2013; Nagakura et al. 2014). Even after a prompt jet is choked, although the profile is modified from the original one, these assumptions may hold. Note that if a prompt jet succeeds in breaking out, it produces a cavity and a late jet (or even a spherical outflow) easily emerges from the ejecta (see also Section 3.1). For homologous ejecta, the velocity is given by $\beta_a = (R_h/R_{ej})\beta_{ej}$, where R_h, $R_{ej} = \beta_{ej} c(t + t_{lag})$, and β_{ej} are the jet head position and the radius and velocity of ejecta edge, respectively. We set the origin of time t as the jet-launching time, which is t_{lag} after the merger. The density is given by

$$\rho_a = \frac{M_{ej}}{4\pi R_{ej}^3} f \left(\frac{R_h}{R_{ej}}\right)^{-k} \quad \text{for} \quad R_{in} \leqslant R \leqslant R_{ej}, \tag{3}$$

$$f = \begin{cases} \dfrac{3-k}{1-\left(\frac{\beta_{esc}}{\beta_{ej}}\right)^{3-k}} & k \neq 3, \\ \dfrac{1}{\ln(\beta_{ej}/\beta_{esc})} & k = 3, \end{cases} \tag{4}$$

where M_{ej} is the ejecta mass. The inner boundary is set by the innermost unbound ejecta at the jet launch as

$$\beta_{esc} = \left(\frac{GM_c\beta_{ej}}{c^2 R_{ej}}\right)^{1/3} \simeq 0.023 \left(\frac{t_{lag}}{\mathrm{s}}\right)^{-1/3} \left(\frac{M_c}{2.6\,M_\odot}\right)^{1/3}, \tag{5}$$

where G and M_c are the gravitational constant and the merger-remnant mass, respectively.

The cocoon pressure determines whether the jet is collimated or conical. The jet cross section is given as

$$\Sigma_j = \begin{cases} \pi\theta_j^2 R_h^2 & \text{conical jet}, \\ \dfrac{L_j\theta_j^2}{4cP_c} & \text{collimated jet}. \end{cases} \tag{6}$$

The cocoon pressure is given by

$$P_c = \frac{E_c}{3V_c} = \frac{\int L_j(1-\beta_h)dt}{\pi R_c^2 R_h}, \tag{7}$$

where the cocoon is radiation-pressure dominated and conical with a height R_h and radius R_c. The cocoon radius is obtained by integrating the cocoon's lateral-expansion velocity of (Begelman & Cioffi 1989)

$$\beta_a = \sqrt{\frac{P_c}{\bar{\rho}_a c^2}}, \tag{8}$$

where $\bar{\rho}_a$ is the cocoon's mean density. When a converging position of the jet's collimation shock (Komissarov & Falle 1997)

$$\hat{z} = \sqrt{\frac{L_j}{\pi c P_c}} \tag{9}$$

is lower than the jet head $R_h \gtrsim \hat{z}$, the jet is collimated.

We integrate the above equations numerically and obtain the jet breakout time t_{br} for various constant jet luminosities. Because Equation (1) overestimates the jet head velocity for $\tilde{L} \lesssim 1$ compared with numerical simulations (Mizuta & Ioka 2013; Harrison et al. 2018), we correct Equation (1) in line with Harrison et al. (2018). We also modify the collimation condition to $R_h \gtrsim \hat{z}/2$ to get a continuous jet cross section.

In Figure 2, we show the result. Each thick red curve shows the breakout time for each lag time. The other parameters are fixed as $\beta_{ej} = 0.3$, $\theta_j = 15^\circ \simeq 0.26$ rad, $M_{ej} = 10^{-2}\,M_\odot$, and $k = 2$. We convert the jet luminosity to the radiation luminosity by adopting an efficiency of $\epsilon_\gamma = 0.1$ as $L_{\gamma,iso} = \epsilon_\gamma L_{j,iso}$. The ejecta velocity and mass are motivated by numerical simulations (Hotokezaka et al. 2013) and the observations of the macronova in GW170817 (e.g., Coulter et al. 2017; Utsumi et al. 2017). The opening angle is based on the observations of sGRBs (Fong et al. 2015), while the observed value may be different from the jet-injection angle. The index $k = 2$ is relevant for wind-like ejecta and a larger indices give shorter breakout times. The thin red curve shows the result for conical jets with $t_{lag} = 1$ s, which give conservative (longer) breakout times. The emission timescale t_{em} and isotropic luminosity of observed sGRBs' emissions are plotted. As the observed sGRBs have successful prompt jets, we can regard the observed emission timescales as engine-working timescales, which ensure that the engine activity (jet launching) duration is long enough for a delayed breakout, $t_{engine} \gtrsim t_{em}$.

For a large jet luminosity (e.g., $L_{j,iso} \gtrsim 10^{51}$ erg s^{-1} for $t_{lag} = 1$ s), the breakout time is smaller than the lag time $t_{br} \lesssim t_{lag}$ and insensitive to the jet luminosity. This is because a large jet luminosity gives a large jet parameter $\tilde{L} \gtrsim 1$ and a jet head velocity becomes almost independent of the jet luminosity $\beta_h \sim 1$. The breakout time is evaluated by equating the jet head radius $\beta_h ct$ and ejecta radius $\beta_{ej} c(t + t_{lag})$ as (Murguia-Berthier et al. 2014),

$$t_{br} \sim \frac{\beta_{ej} t_{lag}}{\beta_h - \beta_{ej}}. \tag{10}$$

With $\beta_h = 1$ and $\beta_{ej} = 0.3$, this equation reasonably reproduces our result as $t_{br} \simeq 0.4\,\mathrm{s}\,t_{lag,0}$. Hereafter, we use the convention $Q_x = Q/10^x$ (cgs). A shorter breakout time than a

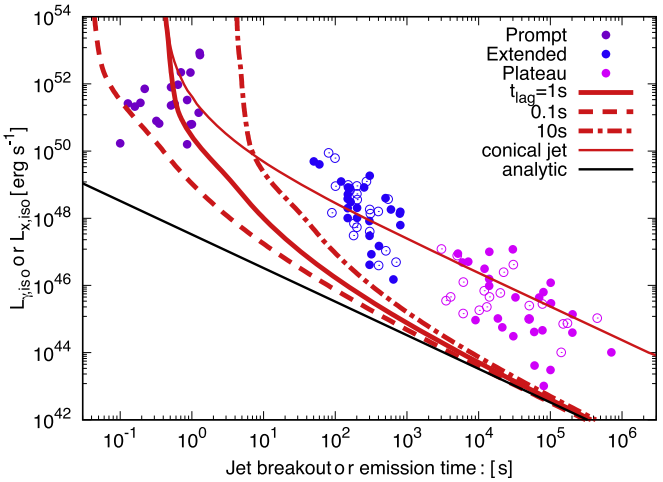

Figure 2. Jet breakout times for various jet luminosities. Thick red dashed, solid, and dashed–dotted curves show the breakout times for lag times $t_{\rm lag} = 0.1$, 1, and 10 s, respectively. The other parameters are $\beta_{\rm ej} = 0.3$, $\theta_{\rm j} = 15^\circ$, $M_{\rm ej} = 10^{-2}\,M_\odot$, and $k = 2$. The jet and radiation luminosities are related as $L_{\gamma,\rm iso} = \epsilon_\gamma L_{\rm j,iso}$ and $\epsilon_\gamma = 0.1$. Thin red solid curve denotes the result for a conical jet ($t_{\rm lag} = 1$ s). The black line shows an analytical formula (Equation (26)). The data points are taken from Zou et al. (2018; for prompt), and Kisaka et al. (2017; extended and plateau emissions). Open circles show the events with unknown redshift (assumed $z = 0.72$).

lag time enables us to regard the envelope as static. In particular, the jet head velocity is constant for the index of $k = 2$, which we assumed to derive Equation (10).

For a small jet luminosity, the jet breakout time gets longer than Equation (10) due to a small jet head velocity. After the lag time, the expansion of ejecta affects the jet head dynamics by reducing the ejecta density and accelerating the jet head (see Equation (2)). A much longer breakout time than the lag time is inversely proportional to the jet luminosity $t_{\rm br} \propto L_{\rm j,iso}^{-1}$. There is a critical energy for a jet to break out of ejecta (Duffell et al. 2018). For a conical jet, this energy is simply given by the ejecta energy $M_{\rm ej}(c\beta_{\rm ej})^2/2 \gtrsim E_{\rm j,iso} \sim L_{\rm j,iso}t$, which reasonably reproduces our result $t \gtrsim 10^2\,{\rm s}\,M_{\rm ej,-2}\beta_{\rm ej,-0.5}^2 L_{\gamma,\rm iso,48}^{-1}$. For a collimated jet with a small ejecta mass in front of the jet head, the required energy is smaller. In the Appendix, we derive an analytical scaling law (Equation (26) and the black line in Figure 2). Note that unless the ejecta expansion is taken into account precisely, the breakout time is significantly overestimated except for the parameter dependence (compare Kimura et al. 2018).

In particular, the jet breakout time for a small jet luminosity should be compared with emission timescales of extended ($t_{\rm em} \sim 10^{2-3}$ s) and plateau emissions ($t_{\rm em} \sim 10^{4-5}$ s). These emission times are longer than the required breakout time and guarantee that if these emissions are produced by jets, the jets can break out of ejecta.

3. Observational Prospects

We discuss the observational prospects of the delayed breakout events. In the following, we mainly consider that a late jet producing an extended emission breaks out. By combining a GW observation and follow-ups, we can check whether or not a delayed jet breakout occurs for a binary merger. First, such a combination tells us whether or not the event is on-axis (Abbott et al. 2017; Finstad et al. 2018; Mandel 2018). For an on-axis event, a detection of prompt γ-rays tells us the fate of its prompt jet. If we detect not a prompt emission but an extended (plateau) emission-like signature i.e., a flat light curve up to $\sim 10^{2-3}$ s (10^{4-5} s) and an abrupt shut down, it strongly supports the theory that the late-time jet does punch out a hole in the ejecta. Therefore, we should set X-ray detectors to the merger event regardless of whether or not prompt γ-rays are detected. In particular, because plateau emissions last for a very long time, they can be a good target for X-ray detectors such as the *Swift* X-ray Telescope (XRT) and *MAXI* (Nakamura et al. 2014; Kisaka et al. 2017).

3.1. A Probe of Late-time Engine Activity in Binary NS Mergers

Delayed-jet-breakout events can be a probe to study what powers have extended and plateau emissions. Currently, the origin of these long-lasting emissions is controversial, as there are two representative models. One is the magnetar model (Metzger et al. 2008; Bucciantini et al. 2012; Gompertz et al. 2013, 2014; Rowlinson et al. 2013; Gibson et al. 2017), where a long-lived magnetar powers energetic outflows through the spin-down or propeller effect. The outflows dissipate energy and power the emissions. The other is the black hole (BH) model (Barkov & Pozanenko 2011; Nakamura et al. 2014; Kisaka & Ioka 2015), in which the emissions are produced by jets from a BH and accretion disk system fueled by fallback matter (Rosswog 2007).

The delayed jet breakout requires a jet (or a collimated outflow), so its detection is evidence that the extended or plateau emission is produced by a jet. Some magnetar models explain long-lasting emissions by rather isotropic magnetar winds. The isotropic outflows cannot break out of ejecta by themselves or produce detectable signals without a hole punched out by a prompt jet. Therefore, the delayed jet breakout strongly supports a BH jet or a mechanism to collimate isotropic magnetar winds (Bucciantini et al. 2012).

The jet eventually collides with the interstellar medium (ISM) and produces an afterglow. The total kinetic energy of the late jet can be comparable to that of prompt jets in ordinary sGRBs. However, its initial Lorentz factor may be lower than that of normal sGRBs, which causes a different afterglow emission. Such a jet decelerates at a longer timescale, and its afterglow peaks at $t_{\rm dec} \sim 3 \times 10^5\,{\rm s}\,E_{\rm j,iso,51}^{1/3} n_{-4}^{-1/3}\Gamma_1^{-8/3}$, where Γ and n are the initial Lorentz factor and the ISM density (Lamb & Kobayashi 2016). While X-ray and optical afterglows may be dimmer than the following plateau and macronova emissions, an identification of their peaks can be a probe of the Lorentz factor of the late-time jet.

3.2. Event Rate

We estimate the event rate of the delayed jet breakout. The binary–NS merger rate is evaluated as $\mathcal{R}_{\rm NSM} \simeq 1550^{+3220}_{-1220}\,{\rm Gpc^{-3}\,yr^{-1}}$ by the observation of GW170817 (Abbott et al. 2017). The merger rate for on-axis events is estimated by assuming the jet opening angle to be

$$\mathcal{R}_{\rm on} \simeq \frac{\theta_{\rm j}^2}{2}\mathcal{R}_{\rm NSM} \simeq 54^{+110}_{-42}\,{\rm Gpc^{-3}\,yr^{-1}}\left(\frac{\theta_{\rm j}}{0.26\,{\rm rad}}\right)^2. \quad (11)$$

The central value is larger than the local sGRB rate of $\simeq 4.1\,{\rm Gpc^{-3}\,yr^{-1}}$ (Wanderman & Piran 2015), and supports the hypothesis that many merger events produce choked jets. For the Laser Interferometer Gravitational-Wave Observatory's

(LIGO)'s full sensitivity, the detectable range of on-axis binary–NS mergers is $d_{\rm L} \simeq 1.6 \times 200\,{\rm Mpc}$, where the factor 1.6 accounts for an enhancement of GWs (Kochanek & Piran 1993), and the comoving volume is $V_{\rm com} \simeq 1.1 \times 10^{-1}\,{\rm Gpc}^3$. The on-axis event rate for the observation by LIGO is evaluated as

$$N_{\rm on} = V_{\rm com}\mathcal{R}_{\rm on} \simeq 6.0^{+12}_{-4.6}\,{\rm yr}^{-1}. \quad (12)$$

The fraction of the delayed-jet-breakout events to the total on-axis events (we denote $f_{\rm delay}$) is constrained by the current sky monitors in X-rays and γ-rays. We adopt a luminosity and duration of a late-time jet as $L_{\rm X,iso} = 10^{48}\,{\rm erg\,s^{-1}}$ and $t_{\rm em} = 300\,{\rm s}$ as fiducial values. A detector with a sensitivity $f_{\rm sen}$ can be triggered by the jet inside the luminosity distance of $d_{\rm L} = (L_{\rm X,iso}/4\pi f_{\rm sen})^{1/2} \simeq 0.94\,{\rm Gpc}\,L^{1/2}_{\rm X,iso,48} f^{-1/2}_{\rm sen,-8}$. We estimate the detection rate of the extended emissions in delayed jet breakouts by *Swift* Burst Alert Telescope (BAT) and *MAXI* Gas Slit Camera (GSC).

BAT has a sensitivity $f_{\rm sen} \sim 10^{-8}\,{\rm erg\,s^{-1}\,cm^{-2}}$ and field of view (FOV) 1.4 str. The detection horizon is $d_{\rm L} \simeq 0.94\,{\rm Gpc}$ ($V_{\rm com} \simeq 2.1\,{\rm Gpc}^3$), and the sky coverage is $1.4/4\pi \simeq 0.11$. The detection rate is $N_{\rm BAT} \simeq 0.1 \times 0.11 \times V_{\rm com} f_{\rm delay}\mathcal{R}_{\rm on} \simeq 1.3^{+2.6}_{-0.98}\,{\rm yr}^{-1} f_{\rm delay}$, where we take that BAT has ever detected only ~10% of extended emissions (Kisaka et al. 2017) into account. This implies that some soft-long GRBs detected by BAT may be the extended emissions in the delayed jet breakouts. These events do not accompany supernova signatures.

MAXI has a sensitivity $f_{\rm sen} \sim 10^{-9}\,{\rm erg\,s^{-1}\,cm^{-2}}$ for soft bands (2–30 keV) and FOV $7.3 \times 10^{-2}\,{\rm str}$ (Sugizaki et al. 2011). The horizon and sky coverage are evaluated as $d_{\rm L} \simeq 3.0\,{\rm Gpc}$ ($V_{\rm com} \simeq 32\,{\rm Gpc}^3$) and $\simeq 5.8 \times 10^{-3}$, respectively. The detection rate is $N_{MAXI} \simeq 0.0058 \times V_{\rm com} f_{\rm delay}\mathcal{R}_{\rm on} \simeq 10.0^{+21}_{-7.8}\,{\rm yr}^{-1} f_{\rm delay}$. This value also suggests that some long GRBs detected by *MAXI* are extended emissions in delayed-jet events. Actually, some GRBs are detected only by *MAXI* and their detection rate is $\sim 5\,{\rm yr}^{-1}$ (Serino et al. 2014).[9] Therefore, *MAXI* constrains the fraction of delayed events as $f_{\rm delay} \lesssim 0.5$ for the central value. Interestingly, for the lower value of $\mathcal{R}_{\rm NSM}$, the fraction is not constrained due to its small event rate. With the on-axis merger rate (Equation (12)), we expect that the rate of delayed jet breakouts coincident with GWs is at most $\sim$1–3 $\,{\rm yr}^{-1}\,(\theta_{\rm j}/0.26\,{\rm rad})^2$.[10] Future wide-field X-ray monitors such as *ISS-Lobster* (Camp et al. 2013) and *Einstein Probe* (Yuan et al. 2015) will detect delayed events or constrain $f_{\rm delay}$ more tightly. We also remark that newly discovered X-ray transients (Bauer et al. 2017) may be related to delayed events.

4. Discussion

In GW170817, although the VLBI observations revealed a relativistic jet with $E_{\rm j,iso} \gtrsim 10^{52}\,{\rm erg}$ (Mooley et al. 2018; Ghirlanda et al. 2018), this jet is not necessarily the origin of the low-luminosity prompt γ-rays (Matsumoto et al. 2018b). We can argue that a prompt jet is choked and the resulting cocoon produces the γ-rays (Kasliwal et al. 2017; Gottlieb et al. 2018; Lazzati et al. 2018), and that the relativistic jet is originated from a delayed breakout. Actually, some extended emissions show $L_{\rm X,iso} \sim 10^{49}\,{\rm erg\,s^{-1}}$ with $t_{\rm em} \sim 10^2\,{\rm s}$ (Figure 2), which suggests a large jet energy of $\sim 10^{52}\,{\rm erg}$. The energetic late jet penetrates the ejecta ~10 s after the prompt jet is choked, and produces a cocoon with $E_{\rm c} \sim 10^{51}\,{\rm erg}$. Interestingly, this cocoon's cooling emission reproduces the observed macronova in the first few days (Matsumoto et al. 2018a). Future GW observations will test this possibility.

In a delayed jet breakout, we have a chance to observe the moment that the late jet emerges from the ejecta. When the jet head reaches the ejecta edge, it may produce a shock-breakout emission (Gottlieb et al. 2018). Even if a merger event occurs outside of the FOV of γ-ray telescopes, the detection of this breakout signature may support the delayed jet breakout.

The delayed-breakout events can be a source of neutrinos. A choked prompt jet can be a powerful neutrino emitter (Kimura et al. 2018). Moreover, a delayed jet emits neutrinos efficiently if it has a low Lorentz factor (Kimura et al. 2017). Detections of these neutrinos can constrain the Lorentz factors and the baryon loading of these jets.

Lamb & Kobayashi (2016) proposed another scenario where on-axis binary–NS mergers do not produce γ-rays. They consider that a low-Lorentz-factor prompt jet breaks out of ejecta but does not emit γ-rays due to its compactness, and discuss the detectability of its afterglow. On the other hand, our scenario predicts that an extended or plateau emission accompanies the merger. In particular, a flat light curve and a sudden drop are unique signatures of a central-engine activity.

Finally, we discuss the breakout condition of prompt jets. A comparison of the breakout time (red curves in Figure 2) with the prompt-emission timescale (purple points) suggests that the lag time should be smaller than $t_{\rm lag} \lesssim 1\,{\rm s}$ to produce a sGRB (see also Murguia-Berthier et al. 2014). For longer lag times, a jet cannot catch up with the ejecta edge within the engine-working time. Note that an event with a short emission time ($t_{\rm em} \ll t_{\rm br}$) does not constrain the lag time because such a burst is produced by a bare breakout $t_{\rm engine} = t_{\rm br} + t_{\rm em} \sim t_{\rm br}$

If each merger event has a similar ejecta velocity and a common lag time, a characteristic breakout time is introduced (see Equation (10)). Intriguingly, Moharana & Piran (2017) found a typical jet breakout time $t_{\rm br} \simeq 0.2$–$0.5\,{\rm s}$. In the collapsar scenario, such a timescale is understood as a time for a jet to reach the progenitor's edge whose size may not change significantly among progenitors (Bromberg et al. 2012). However, binary mergers do not have a characteristic size because ejecta expand. A common lag time introduces such a special length $\sim\beta_{\rm ej} c t_{\rm lag}$ into the systems. Therefore, the typical breakout time may suggest that there is a favored lag time to produce sGRBs, which may be related to the jet-launch mechanism such as the formation of global magnetic fields or a BH.

We thank Motoko Serino for useful comments on the observations by *MAXI*. We are also grateful to Peter Mészáros for helpful comments. This Letter is supported by JSPS Overseas Challenge Program for Young Researchers, Grant-in-Aid for JSPS Research Fellow 17J09895 (T.M.), JSPS Oversea Research Fellowship, and the IGC post-doctoral fellowship program (S.S.K.).

[9] Other X-ray transients might be included in the *MAXI* GRBs, which reduces $f_{\rm delay}$ further. A candidate is shock breakouts of SNe, as they show thermal emissions. Detecting the optical counterparts of *MAXI* GRBs, we can firmly distinguish these events from delayed breakouts.

[10] Note that there is still an uncertainty in the jet opening angle, which affects the event rate. For instance, Beniamini et al. (2018) argued that the merger rate is consistent with the sGRB rate, because they assume a narrower jet-opening angle than ours.

Appendix
Analytical Formula

We derive analytical formulae for jet propagations in homologously expanding media.

A.1. Conical Jet

For a conical jet, the jet parameter is given by

$$\tilde{L} = \frac{L_{\rm j}}{\pi\theta_{\rm j}^2 R_{\rm h}^2 \rho_{\rm a} c^3} = \frac{L_{\rm j}}{\pi \mathcal{A}\theta_{\rm j}^2 c^3} R_{\rm h}^{k-2}, \tag{13}$$

where we define $\rho_{\rm a} = \mathcal{A} R_{\rm h}^{-k}$. For $\tilde{L} \lesssim 1$, we can approximate Equation (1) as $\beta_{\rm h} \simeq \tilde{L}^{1/2} + \beta_{\rm a}$ and rewrite it as

$$t\frac{d(R_{\rm h}/t)}{dt} = c\tilde{L}^{1/2}, \tag{14}$$

where we used $\beta_{\rm a} \simeq R_{\rm h}/t$ for a homologously expanding media at later than $t > t_{\rm lag}$. Due to a term $\beta_{\rm a}$, the left-hand side has a different form than that for static media cases. This gives a different numerical coefficient than a static one. By integrating Equation (14), we obtain a formula

$$R_{\rm h} = \left[\frac{L_{\rm j}}{\mathcal{A}\theta_{\rm j}^2 c}\frac{1}{\pi}\left(\frac{4-k}{k-p-2}\right)^2\right]^{\frac{1}{4-k}} t^{\frac{2}{4-k}} \propto t^{\frac{2-p}{4-k}}, \tag{15}$$

for $2 + p < k < 4$, where the constant p is defined as $\mathcal{A} = \tilde{\mathcal{A}} t^p$. In our model, the quantities are $k = 2$, $\mathcal{A} = M_{\rm ej} f/4\pi R_{\rm ej}{}^{3-k}$, and $p = k - 3$, and give

$$R_{\rm h} = 7.6 \times 10^6 \,{\rm cm}\, M_{\rm ej,-2}^{-1/2} L_{\rm j,iso,45}^{1/2} \beta_{\rm ej,-0.5}^{1/2} (t/{\rm s})^{3/2}. \tag{16}$$

By equating this radius with the ejecta edge $R_{\rm ej} \sim \beta_{\rm ej} ct$, we obtain the critical luminosity for successful jet breakouts as

$$L_{\rm j,iso} \simeq 1.5 \times 10^{51}\,{\rm erg\ s^{-1}}\, M_{\rm ej,-2}\beta_{\rm ej,-0.5}(t/{\rm s})^{-1}. \tag{17}$$

A.2. Collimated Jet

Next, we consider a collimated jet. At $t > t_{\rm lag}$, we denote the cocoon radius as $R_{\rm c} = \xi\beta_{\rm c} ct$, where a numerical coefficient ξ is given later. The cocoon pressure is rewritten by using Equations (7) and (8) as

$$P_{\rm c} \simeq \frac{L_{\rm j} t}{3^{\pi}_{3} R_{\rm c}^2 R_{\rm h}} = \frac{L_{\rm j}}{\pi\xi^2\beta_{\rm c}^2 R_{\rm h} c^2 t} = \left(\frac{L_{\rm j}\bar{\rho}_{\rm a}}{\pi\xi^2 R_{\rm h} t}\right)^{1/2}. \tag{18}$$

The jet parameter is given as

$$\tilde{L} = \frac{L_{\rm j}}{\frac{L_{\rm j}\theta_{\rm j}^2}{4cR_{\rm c}^2}\rho_{\rm a} c^3} = \left(\frac{L_{\rm j}}{\mathcal{A}\theta_{\rm j}^4 c^4}\frac{16\varrho}{\pi\xi^2}\frac{R_{\rm h}^{k-1}}{t}\right)^{1/2}, \tag{19}$$

where we use $\bar{\rho}_{\rm a} = \varrho\rho_{\rm a}$ and $\varrho = 3/(3-k)$ for a conical cocoon. By substituting this for Equation (14), we obtain

$$R_{\rm h} = \left[\frac{L_{\rm j}}{\mathcal{A}\theta_{\rm j}^4}\frac{16\varrho}{\pi\xi^2}\left(\frac{5-k}{k-2-p}\right)^4\right]^{\frac{1}{5-k}} t^{\frac{3}{5-k}} \propto t^{\frac{3-p}{5-k}}, \tag{20}$$

for $p - 2 < k < 5$. The cocoon velocity is given as

$$\beta_{\rm c} \propto (P_{\rm c}/\bar{\rho}_{\rm a})^{1/2} \propto (\rho_{\rm a} R_{\rm h} t)^{-1/4} \propto (t^{p+1} R_{\rm h}^{1-k})^{-1/4} \propto t^{\frac{p+2-k}{k-5}}, \tag{21}$$

which gives the coefficient as $\xi = (5-k)/(3-p)$. Finally, we get analytical expressions as

$$R_{\rm h} = N_{\rm s}^{\frac{5}{5-k}}\left[\frac{3L_{\rm j}}{\mathcal{A}\theta_{\rm j}^4}\frac{2^4}{\pi(3-p)^2}\frac{(5-k)^2}{(3-k)}\left(\frac{3-p}{p+2-k}\right)^4\right]^{\frac{1}{5-k}} t^{\frac{3}{5-k}}, \tag{22}$$

$$\beta_{\rm h} = N_{\rm s}^{\frac{5}{5-k}}\left[\frac{3L_{\rm j}}{\mathcal{A}\theta_{\rm j}^4}\frac{2^4(3-p)^{3-k}}{\pi}\frac{(5-k)^{k-3}}{(3-k)} \times \left(\frac{3-p}{p+2-k}\right)^4\right]^{\frac{1}{5-k}} \frac{t^{\frac{k-2}{5-k}}}{c}, \tag{23}$$

where we introduce a correction factor $N_{\rm s}$(=0.35 for $\tilde{L} < 1$) given by Harrison et al. (2018). The time dependences are the same as Margalit et al. (2018). We compare these forms with Equations (A2) and (A3) in Harrison et al. (2018). They do not consider the time-dependent $\mathcal{A}$, which modifies numerical coefficients. Furthermore, in expanding media, the jet head velocity is determined by not only $\tilde{L}$ but also $\beta_{\rm a}$ (see Equation (1)). In particular, Equation (14) gives another factor $[(3-p)/(p+2-k)]^4$.

For our case, the jet head velocity and radius are given by

$$\beta_{\rm h} = 3.0 \times 10^{-2} M_{\rm ej,-2}^{-1/3} L_{\rm j,iso,45}^{1/3} \beta_{\rm ej,-0.5}^{1/3} \theta_{\rm ej,-0.5}^{-2/3} \times (t/{\rm s})^{1/3}\left(\frac{N_{\rm s}}{0.35}\right)^{5/3}, \tag{24}$$

$$R_{\rm h} = 6.8 \times 10^8\,{\rm cm}\, M_{\rm ej,-2}^{-1/3} L_{\rm j,iso,45}^{1/3} \beta_{\rm ej,-0.5}^{1/3} \theta_{\rm ej,-0.5}^{-2/3} \times (t/{\rm s})^{4/3}\left(\frac{N_{\rm s}}{0.35}\right)^{5/3}, \tag{25}$$

and the critical luminosity is given by

$$L_{\rm j,iso} = 5.4 \times 10^{48}\,{\rm erg\ s^{-1}}\, M_{\rm ej,-2}\beta_{\rm ej,-0.5}^2 \theta_{\rm ej,-0.5}^2 \times (t/{\rm s})^{-1}\left(\frac{N_{\rm s}}{0.35}\right)^{-5}. \tag{26}$$

It should be noted that the different numerical factors introduce a large difference in the critical luminosity. Actually, Kimura et al. (2018) used the equations in Harrison et al. (2018) and obtained a much larger critical luminosity than Equation (26). The discrepancy between ours and theirs are reasonably attributed to the different numerical factor that they adopted as $[(3-p)/3]^2[(p+2-k)/(3-p)]^4 \simeq 7 \times 10^{-3}$.

ORCID iDs

Shigeo S. Kimura https://orcid.org/0000-0003-2579-7266

References

Abbott, B. P., Abbott, R., Abbott, T. D., et al. 2017, PhRvL, 119, 161101
Barkov, M. V., & Pozanenko, A. S. 2011, MNRAS, 417, 2161
Bauer, F. E., Treister, E., Schawinski, K., et al. 2017, MNRAS, 467, 4841
Begelman, M. C., & Cioffi, D. F. 1989, ApJL, 345, L21
Beniamini, P., Petropoulou, M., Barniol Duran, R., & Giannios, D. 2018, arXiv:1808.04831
Berger, E. 2014, ARA&A, 52, 43
Bromberg, O., Nakar, E., Piran, T., & Sari, R. 2011, ApJ, 740, 100
Bromberg, O., Nakar, E., Piran, T., & Sari, R. 2012, ApJ, 749, 110

Bucciantini, N., Metzger, B. D., Thompson, T. A., & Quataert, E. 2012, MNRAS, 419, 1537
Camp, J., Barthelmy, S., Blackburn, L., et al. 2013, ExA, 36, 505
Coulter, D. A., Foley, R. J., Kilpatrick, C. D., et al. 2017, Sci, 358, 1556
Duffell, P. C., Quataert, E., Kasen, D., & Klion, H. 2018, arXiv:1806.10616
Eichler, D., Livio, M., Piran, T., & Schramm, D. N. 1989, Natur, 340, 126
Finstad, D., De, S., Brown, D. A., Berger, E., & Biwer, C. M. 2018, ApJL, 860, L2
Fong, W., Berger, E., Margutti, R., & Zauderer, B. A. 2015, ApJ, 815, 102
Ghirlanda, G., Salafia, O. S., Paragi, Z., et al. 2018, arXiv:1808.00469
Gibson, S. L., Wynn, G. A., Gompertz, B. P., & O'Brien, P. T. 2017, MNRAS, 470, 4925
Gompertz, B. P., O'Brien, P. T., & Wynn, G. A. 2014, MNRAS, 438, 240
Gompertz, B. P., O'Brien, P. T., Wynn, G. A., & Rowlinson, A. 2013, MNRAS, 431, 1745
Gottlieb, O., Nakar, E., Piran, T., & Hotokezaka, K. 2018, MNRAS, arXiv:1710.05896
Harrison, R., Gottlieb, O., & Nakar, E. 2018, MNRAS, 477, 2128
Hotokezaka, K., Kiuchi, K., Kyutoku, K., et al. 2013, PhRvD, 87, 024001
Ioka, K., Kobayashi, S., & Zhang, B. 2005, ApJ, 631, 429
Kasliwal, M. M., Nakar, E., Singer, L. P., et al. 2017, Sci, 358, 1559
Kimura, S. S., Murase, K., Bartos, I., et al. 2018, arXiv:1805.11613
Kimura, S. S., Murase, K., Mészáros, P., & Kiuchi, K. 2017, ApJL, 848, L4
Kisaka, S., & Ioka, K. 2015, ApJL, 804, L16
Kisaka, S., Ioka, K., & Sakamoto, T. 2017, ApJ, 846, 142
Kochanek, C. S., & Piran, T. 1993, ApJL, 417, L17
Komissarov, S. S., & Falle, S. A. E. G. 1997, MNRAS, 288, 833
Lamb, G. P., & Kobayashi, S. 2016, ApJ, 829, 112
Lazzati, D., Perna, R., Morsony, B. J., et al. 2018, PhRvL, 120, 241103
Mandel, I. 2018, ApJL, 853, L12
Margalit, B., Metzger, B. D., Thompson, T. A., Nicholl, M., & Sukhbold, T. 2018, MNRAS, 475, 2659
Matsumoto, T., Ioka, K., Kisaka, S., & Nakar, E. 2018a, ApJ, 861, 55
Matsumoto, T., Nakar, E., & Piran, T. 2018b, arXiv:1807.04756
Matzner, C. D. 2003, MNRAS, 345, 575
Metzger, B. D., Quataert, E., & Thompson, T. A. 2008, MNRAS, 385, 1455
Mizuta, A., & Ioka, K. 2013, ApJ, 777, 162
Moharana, R., & Piran, T. 2017, MNRAS, 472, L55
Mooley, K. P., Deller, A. T., Gottlieb, O., et al. 2018, arXiv:1806.09693
Murguia-Berthier, A., Montes, G., Ramirez-Ruiz, E., De Colle, F., & Lee, W. H. 2014, ApJL, 788, L8
Nagakura, H., Hotokezaka, K., Sekiguchi, Y., Shibata, M., & Ioka, K. 2014, ApJL, 784, L28
Nakamura, T., Kashiyama, K., Nakauchi, D., et al. 2014, ApJ, 796, 13
Nakar, E. 2007, PhR, 442, 166
Norris, J. P., & Bonnell, J. T. 2006, ApJ, 643, 266
Perley, D. A., Metzger, B. D., Granot, J., et al. 2009, ApJ, 696, 1871
Rosswog, S. 2007, MNRAS, 376, L48
Rowlinson, A., O'Brien, P. T., Metzger, B. D., Tanvir, N. R., & Levan, A. J. 2013, MNRAS, 430, 1061
Serino, M., Sakamoto, T., Kawai, N., et al. 2014, PASJ, 66, 87
Sugizaki, M., Mihara, T., Serino, M., et al. 2011, PASJ, 63, S635
Utsumi, Y., Tanaka, M., Tominaga, N., et al. 2017, PASJ, 69, 101
Wanderman, D., & Piran, T. 2015, MNRAS, 448, 3026
Yuan, W., Zhang, C., Feng, H., et al. 2015, arXiv:1506.07735
Zou, Y.-C., Wang, F.-F., Moharana, R., et al. 2018, ApJL, 852, L1